Carbohydrate Polymers 86 (2011) 903–909

Contents lists available at ScienceDirect

Carbohydrate Polymers

journal homepage: www.elsevier.com/locate/carbpol

Graphene oxide/cellulose composite using NMMO monohydrate

Chan-Jun Kim, Waliullah Khan, Dong-Hun Kim, Kwang-Soo Cho, Soo-Young Park*

Department of Polymer Science, Kyungpook National University, #1370 Sangyuk-dong, Buk-gu, Daegu 702-701, South Korea

ARTICLE INFO

Article history:
Received 1 February 2011
Received in revised form 4 May 2011
Accepted 23 May 2011
Available online 31 May 2011

Keywords:
Graphene oxide
Cellulose
Composite
NMMO
Electrical conductivity

ABSTRACT

Graphene oxide (GO)/cellulose composite films were prepared by using an N-methylmorpholine-N-oxide (NMMO) monohydrate solvent. NMMO was an excellent dispersing agent for the GO as well as an environmentally friendly solvent for cellulose. The presence of a small amount of the GO significantly changed the rheological properties of the GO/cellulose/NMMO dope, and the thermal, electrical, and mechanical properties of the composite films. The viscosity of the GO/cellulose/NMMO dope increased significantly when a small amount of the GO was added into the dope. Thermal annealing of the composite films at 250 °C removed the oxygen containing groups of the GO in the cellulose matrix and led to improvement of the electrical conductivity of the composite films. The interactions between the GO and cellulose made the composite films strong but brittle as a result of adding a small amount of the GO into the composite.

1. Introduction

Cellulose is a renewable, biodegradable, biocompatible and an almost inexhaustible source of raw materials that can be used to replace petrochemical compounds in many cases (Klemm, Heublein, Fink, & Bohn, 2005). However, cellulose is difficult to process in a solution or melted state, because of its large proportions of intra- and inter-molecular hydrogen bonds. Thus, the viscose process for the production of rayon requires environmentally hazardous toxic chemicals such as sulfuric acid (H_2SO_4) and carbon disulfide (CS_2). The lyocell process made an industrial breakthrough as an environmentally friendly alternative to the viscose process, whereby cellulose is regenerated from a solution in N-methylmorpholine-N-oxide (NMMO) monohydrate which is non-toxic and recoverable. Due to its strong N–O dipole of NMMO, NMMO monohydrate can dissolve cellulose without cell activation or derivatization.

Graphene is a two-dimensional single layer of sp^2-bonded carbons with a thickness of one atomic layer (~1 nm). It has recently attracted increasing attention because of its peculiar electronic properties, such as the quantum Hall effect (Zhang, Tan, Stormer, & Kim, 2005), two-dimensional Dirac fermions (Novoselov et al., 2005), ambipolar electric field effect, its ballistic conduction of charge carriers (Novoselov et al., 2004), and its tunable band gap (Han, Oezyilmaz, Zhang, & Kim, 2007) with extraordinary thermal and mechanical properties that rival in-plane values of graphite (Balandin et al., 2008; Castro, Guinea, Peres, Novoselov, & Geim, 2009; Geim & Novoselov, 2007; Lee, Wei, Kysar, & Hone, 2008). These superior properties open various promising potential applications in the fields of composites (Ramanathan et al., 2008; Stankovich et al., 2006a), transparent conductive films (Eda, Fanchini, & Chhowalla, 2008; Wang, Zhi, & Mullen, 2008), lithium-ion batteries (Yoo et al., 2008), super capacitors (Vivekchand, Rout, Subrahmanyam, Govindaraj, & Rao, 2008), organic photovoltaic cells (Liu et al., 2008; Wang et al., 2008b), electron field emitters (Wu et al., 2009), field effect transistors (Mori, Kikuzawa, & Takeuchi, 2008), and ultrasensitive sensors (Schedin et al., 2007). One possible way to harness graphene's exceptional properties would be to incorporate graphene into a matrix material as a second-phase filler to substantially enhance the electric, thermal, and mechanical properties. Composite materials employing carbon-based materials such as carbon-nanotube (CNT), graphene, and fullerene have been explored. However, at present, CNT has dominated carbon-based composites for use as filler even though its intrinsic bundling, impurities from the catalysts, and high costs, especially for single-walled CNT (SWCNT), have all hampered its applications. Graphene/polymer composites have recently been focused on because the properties of graphene are comparable to those of CNT or superior in some properties such as thermal conductivity. Additionally, the price of graphene is relatively cheaper than SWCNT. It was reported that a graphene/polystyrene composite exhibits a percolation threshold in electric conductivity at a filler volume fraction as low as 0.1 volume%, which is comparable to those observed in CNT-based composites (Stankovich et al., 2006a), and a conductivity of 0.1 S m^{-1}, which is sufficient for many electrical applications (Chung, 2004). The manufacturing of

* Corresponding author. Tel.: +82 53 950 5630; fax: +82 53 950 6623.
E-mail address: psy@knu.ac.kr (S.-Y. Park).

0144-8617/$ – see front matter © 2011 Elsevier Ltd. All rights reserved.
doi:10.1016/j.carbpol.2011.05.041

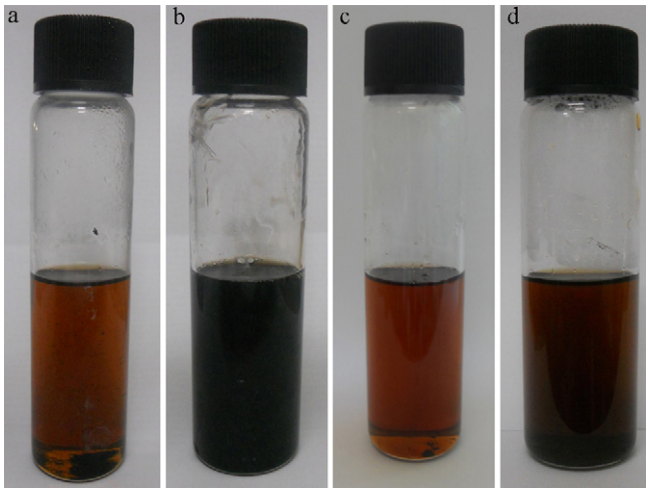

Fig. 1. The images of the dispersion of the GO (a and b) and graphite (c and d) powder (3 mg) in 30 mL NMMO at 95 °C before (a and c) and after (b and d) sonicating them for 30 min in the glass vials.

such composites requires that graphene not only be produced on a sufficient scale but also homogeneously distributed into various matrices in order to maintain the novel properties of graphene in the composites.

Several strategies, such as mechanical cleavage (Novoselov et al., 2004), epitaxial growth on SiC (Berger et al., 2006) or metal substrates (Sutter, Flege, & Sutter, 2008), and chemical exfoliation of graphite (Li, Muller, Gilje, Kaner, & Wallace, 2008; Stankovich et al., 2007; Stankovich, Piner, Nguyen, & Ruoff, 2006), have been developed in order to produce graphene. Among these methods, chemical exfoliation is widely considered as a promising approach for a large-scale inexpensive solution for the production of graphene. The exfoliated carbon sheets can be made through the oxidation of graphite crystals, which would introduce oxygen-containing groups into the graphite gallery followed by complete exfoliation into the sheets of atomic-thickness through either thermal or mechanical treatments (Stankovich et al., 2006b). The oxygenated graphite and its isolated carbon sheet are called graphite oxide and graphene oxide(GO), respectively. The graphene oxide is interconnected by a network of cyclohexane-like units in a chair configuration which are decorated by hydroxyl, epoxy, ether, diol, and ketone groups (Szabo et al., 2006). The presence of these oxygen-containing groups makes the GO strongly hydrophilic and allows it to readily disperse in water (Hirata, Gotou, Horiuchi, Fujiwara, & Ohba, 2004; Hirata, Gotou, & Ohba, 2005; Szabo, Szeri, & Dekany, 2005). The dispersion behavior of the GO in different organic solvents, such as dimethylformamide (DMF), N-methyl-2-pyrrolidone (NMP), ethylene glycol (EG) and tetrahydrofuran (THF), has been studied (Paredes, Villar-Rodil, Martinez-Alonso, & Tascon, 2008).

NMMO can make hydrogen bonds with cellulose as well as graphite (and graphene) oxides. Thus, three components in a solution-blend composite system such as matrix, filler and solvent have hydrogen bonding capability. As a result well-dispersed graphite (and graphene) oxides in cellulose matrix and strong physical hydrogen bonding between matrix and filler can be expected. In this study the GO/cellulose composite films were prepared by using environmentally friendly NMMO monohydrate for dissolving cellulose as well as dispersing the GO. The effects of the well-dispersed GO in the cellulose matrix on the mechanical, thermal, and electrical properties of the composite films were studied.

2. Experimental

2.1. Materials

Cellulose powder (Buckeye Co. V-81 grade, number-averaged molecular weight (M_n) = 1200) and NMMO monohydrate (which was evaporated from 50 wt% aqueous solution of BASF© NMMO) were supplied by Kolon©. The graphite used in this study was purchased from Samjung C&G Inc.© (FP 99.95). The GO was synthesized by using the modified Hummers method. A small amount of flake graphite (4 g) was vigorously stirred for 3 h in a concentrated H_2SO_4 (92 ml) solution of $NaNO_3$ (2 g) and $KMnO_4$ (12 g), washed with a 5 wt% aqueous H_2SO_4 solution, and treated with a 30 wt% aqueous H_2O_2 solution to reduce the residual permanganate and MnO_2 to colorless soluble $MnSO_4$ salts. The GO suspensions were filtered with filter papers and rinsed with distilled water more than 15 times until pH 7 was obtained. The GO powder was obtained after drying it at 60 °C in an oven.

2.2. The GO/cellulose film preparation

NMMO was used in a mono-hydrated state and "NMMO" in this article means NMMO monohydrate. In a glass tube, NMMO was heated to 95 °C in an oil-bath and the GO powders were added into the tube in different amounts. The GO powders in the NMMO solution were dispersed with a tip-type ultra-sonicator (Vibracell, VCX-750 700 W/60 Hz) for 6 h. The cellulose powder (5 wt%) was added into the GO/NMMO solution and mixed with a mechanical stirrer for 2 h. The dispersed composite dope was degassed for 1 h to remove air with an aspirator. The viscous dope was poured on the glass plate and cast into a film by drawing a glass bar over the plate. The gap between the glass bar and the plate was controlled by thick pieces of rolled tape on both end-edges of the glass bar. The film on the plate was immersed into a water bath for a day to remove the NMMO and then dried in a sample holder.

2.3. The pure GO film

The GO film was made from the aqueous GO suspension. 20 mL of the GO powder (4 mg/mL) were sonicated with a tip-type sonicator (Vibracell, VCX-750) for 1 h and then heated at 60 °C in a Teflon-coated Petri dish. After drying completely, the deposited GO film was peeled off from the bottom of the glass. The resultant GO film was ~30 μm thick.

2.4. Characterization

Micrographs of the osmium tetroxide (OsO_4)-coated surface of the fractured GO/cellulose composite films in liquid nitrogen were taken using a Hitachi S-4800 scanning electron microscope (SEM) with an accelerating voltage of 15 kV. Thermo gravimetric analysis (TGA) thermograms of the composite were taken in a TGA-50 (Shimadzu Co.) with a temperature range of 150–500 °C under a nitrogen atmosphere with a scan rate of 10 °C/min. The tensile properties of the composite films were measured with an Instron 4465 (Instron Co.) at room temperature (~18 °C). The length, width, and thickness were 30, 10, and 25 ㎜, respectively. The extension rate was set at 10 mm/min and the load cell was 5 kg. The conductivities of the GO/cellulose composite films were measured at an ambient temperature by a four-point probe method using an HMS-3000 (Ecopia). The dimensions of the samples were about 10 mm (length) × 10 mm (width) × ~0.025 mm (thickness) and their ends were coated with an indium paste to ensure good electrical contact. The instrumental limit of the electrical conductivity is in the range of 10^3 to 10^{-6} S cm^{-1}. Wide-angle X-ray diffraction pat-

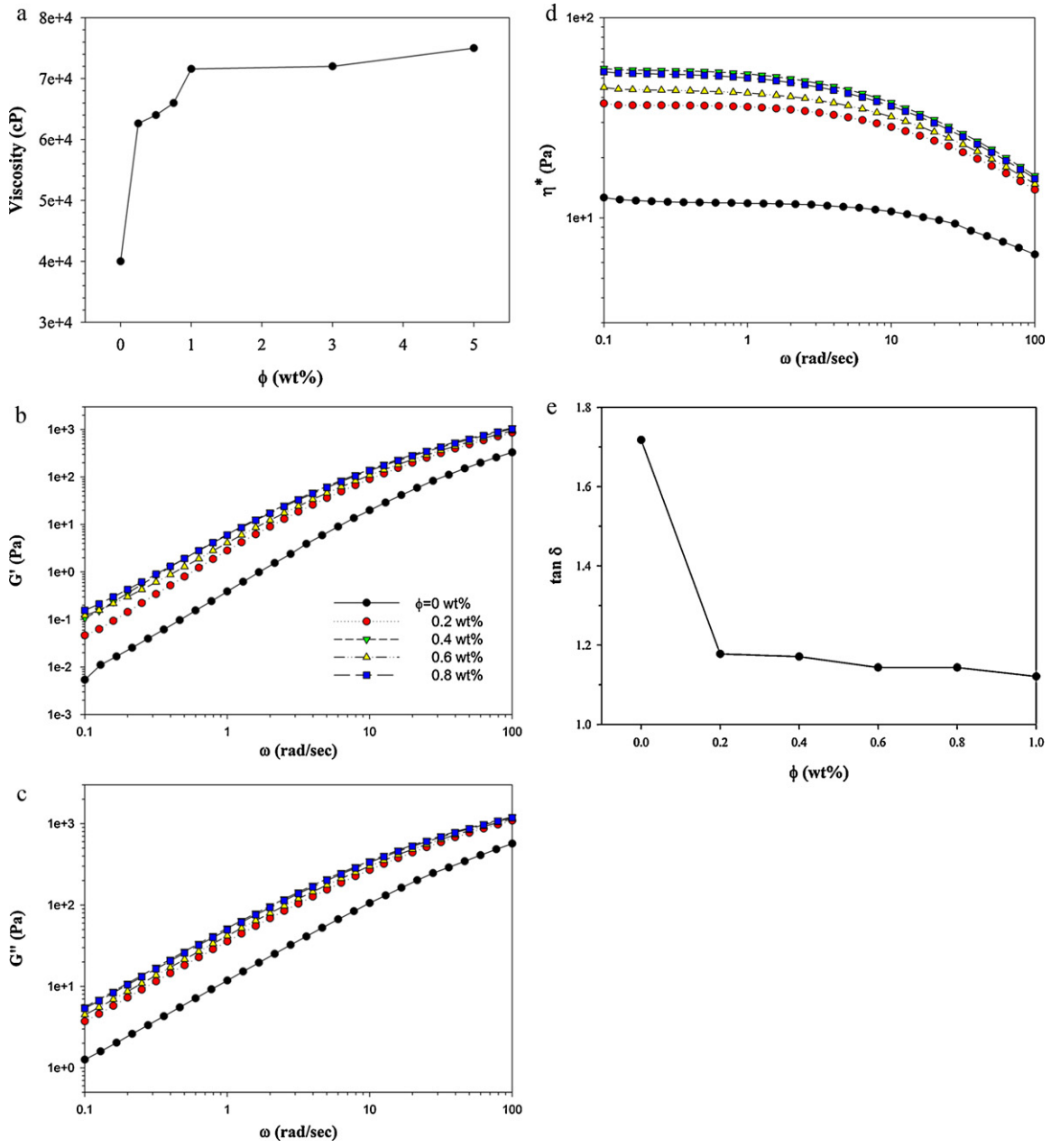

Fig. 2. Rheological properties of the cellulose/GO/NMMO dopes at different ϕ_s; (a) viscosity from Brookfield viscometer; dynamic rheological properties of (b) G', (c) G'', and (d) η^* as a function of ω; (e) tan δ (G''/G') as a function of ϕ; all measurements were done at 95 °C.

terns were recorded on a phosphor image plate (PerkinElmer, Cyclone) by a Statton camera. An Anton-Parr X-ray generator, operated at 40 kV and 50 mA, produced Cu Kα radiation, which was monochromatized with a flat monochromator (Huber model 151). The sample-to-film distance was calibrated by SiO_2 powders. Brookfield viscosity was measured with a spindle NO. 7 at 10 rpm; the model of the Brookfield viscometer was RVDV-II + Pro. The spindle was inserted 7 cm below the surface of the dope in the glass tube, which has dimensions of 5 cm in diameter and 13 cm in depth. Dynamic rheological properties, such as the storage and loss moduli (G', G''), complex viscosity (η^*), and tan δ, were measured with a dynamic viscometer (Haake Mars). The parallel plate (60 mm in diameter) was used for a frequency sweep with a 1 mm gap. Linear viscoelastic region was determined by a dynamic stress sweep; the rheometer used was stress-controlled rather than strain-controlled. Dynamic rheological properties (such as G', G'' and η^*) did not change until ~4 Pa and thus, all dynamic tests were conducted at 2 Pa.

3. Results and discussion

3.1. GO/cellulose/NMMO dope

Fig. 1 shows the images of the dispersion of the GO and graphite powder (3 mg) in 30 mL NMMO at 95 °C before and after sonicating them for 30 min in the glass vial. The GO/NMMO solution became black after sonication (Fig. 1b) indicating that the GO powder was completely dispersed in the NMMO. Any aggregation of the GO powder in NMMO could not be observed after several weeks since the GO powder had been sonicated in NMMO. However, the graphite powder settled at the bottom of the glass tube without a significant change in the color of the solution (Fig. 1d) after

sonication. This result indicates that NMMO was a good dispersion agent for the GO due to the hydrogen bonds between the oxygen-containing groups of the GO and the N–O linkage in the NMMO; the dipole moment of N–O is 4.38 mD and the oxygen in the N–O in NMMO is highly proton-accepting.

The rheological properties of the prepared cellulose/GO/NMMO dopes were measured. The content of the GO in cellulose was denoted as ϕ. Viscoelastic behavior is known to be strongly dependent on filler dispersion and interfacial interactions between fillers and matrix materials. Fig. 2 shows the rheological properties of the cellulose/GO/NMMO dopes at different ϕ_s. Viscosity measured with a Brookfield viscometer at room temperature (Fig. 2a) showed a step-wise increase with an addition of a small amount of the GO at $\phi = 0.25$ wt% and then a slight increase after that. The step-wise increase of viscosity might be due to the interactions between the GO and cellulose by hydrogen bonds, which might already be saturated at low loading of the GO. Fig. 2b and c shows the G' and G'' as a function of dynamic frequency (ω). The G' and G'' step-wise increased at $\phi = 0.25$ wt% at all measured frequency ranges, although the increase of the G' and G'' were almost saturated at $\phi > 0.25$ wt%, similar to the dependence of the Brookfield viscosities on ϕ. The cellulose chains in the dope exhibited typical terminal behavior with the approximate scaling properties of $G' \sim \omega^2$, $G'' \sim \omega$ and $G'' > G'$ at low frequencies. The slopes of the log-log plots in the region of $\omega = 0.1$ to 1 rad/s were 1.71 ± 0.2 and 0.98 ± 0.01 for G' and G'', respectively. Fig. 2e shows the $\tan\delta$ (G''/G') as a function of ϕ at $\omega = 100$ rad/s. The $\tan\delta$ also decreased suddenly at $\phi = 0.25$ wt% indicating that the G' increased more than the G'' by adding a small amount of the GO into the dope. This behavior is also reflected in an increase of elasticity by interactions between the GO and cellulose through hydrogen bonds. Fig. 2d shows the η^* as a function of ω. The η^* at $\phi = 0$ (pure cellulose dope) showed a large Newtonian plateau region, although it decreased as ϕ increased. The decrease of the plateau region might indicate that large-scale polymer chain relaxations in the dope are restrained by the hydrogen bonds between the GO and cellulose. In the cases of percolated polymer melt systems, the η^* (or η) monotonically decreases as ω (or shear rate) increases. For example, no plateau region is observed, the dependence of G' on ω is reduced (becomes flattened), and G' is higher than G'' at low frequency due to a transition from the liquid-like state to the solid-like one (Saeed & Park, 2007a,b; Zhang, Rastogi, Chen, Lippits, & Lemstra, 2006) This non-terminal behavior is attributed to the formation of a mesostructure of filler, i.e., a percolated network structure which restrains the long-range motion of polymer chains. However, the majority of the polymer dope systems is solvent and such the formation of the percolated network structure might not be possible at 5 wt% polymer concentration in NMMO and low loading of the GO (maximum $\phi = 5$ wt% in the work).

3.2. Structure of the GO/cellulose composite

Fig. 3a–d show the beam geometry, two-dimensional X-ray patterns of the GO film, the pure cellulose, and the GO (5 wt%)/cellulose composite films when an X-ray beam was parallel to the film's surface; the direction of the X-ray beam, the vertical and horizontal directions in the two-dimensional X-ray pattern are in Fig. 3a. The two-dimensional X-ray pattern of the pure GO film (Fig. 3b) shows the diffraction peak at $2\theta = 12.2^\circ$ (d-spacing = 7.3 Å) perpendicular to the film's surface (the horizontal direction in Fig. 3b) and the peak at $2\theta = 43^\circ$ (d-spacing = 2.1 Å) parallel to the film's surface (the vertical direction in Fig. 3b). The peak running horizontally is due to the gallery gap of the layered structure of the GO. The peak running vertically is due to the hexagonal in-plane structure of the carbon layer. The gallery gap of the GO film increased as compared to that of the graphite (3.35 Å). How-

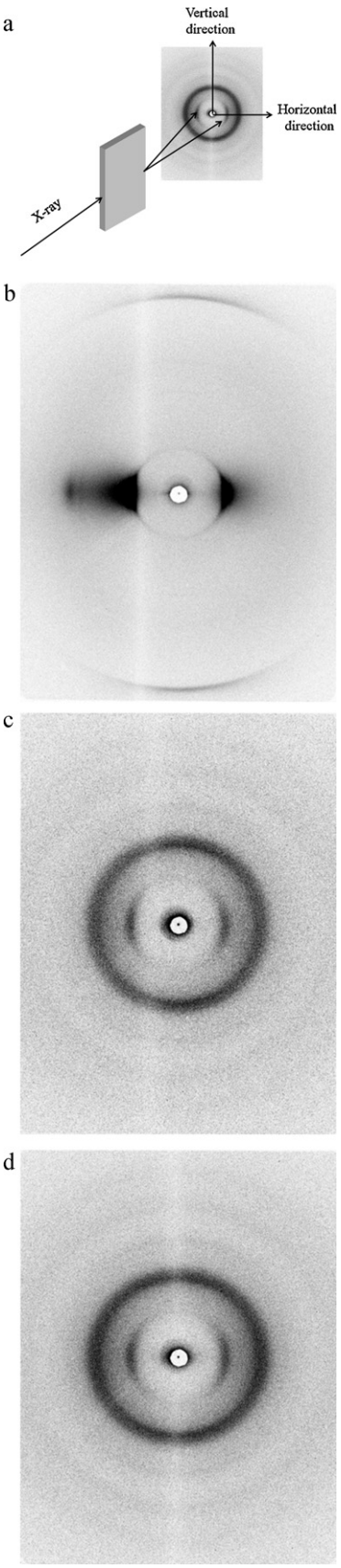

Fig. 3. Geometry of the X-ray beam (a), two-dimensional X-ray patterns of (b) the pure GO film, (c) the pure cellulose film, and (d) the GO (5 wt%)/cellulose composite when an X-ray beam was parallel to the film's surface.

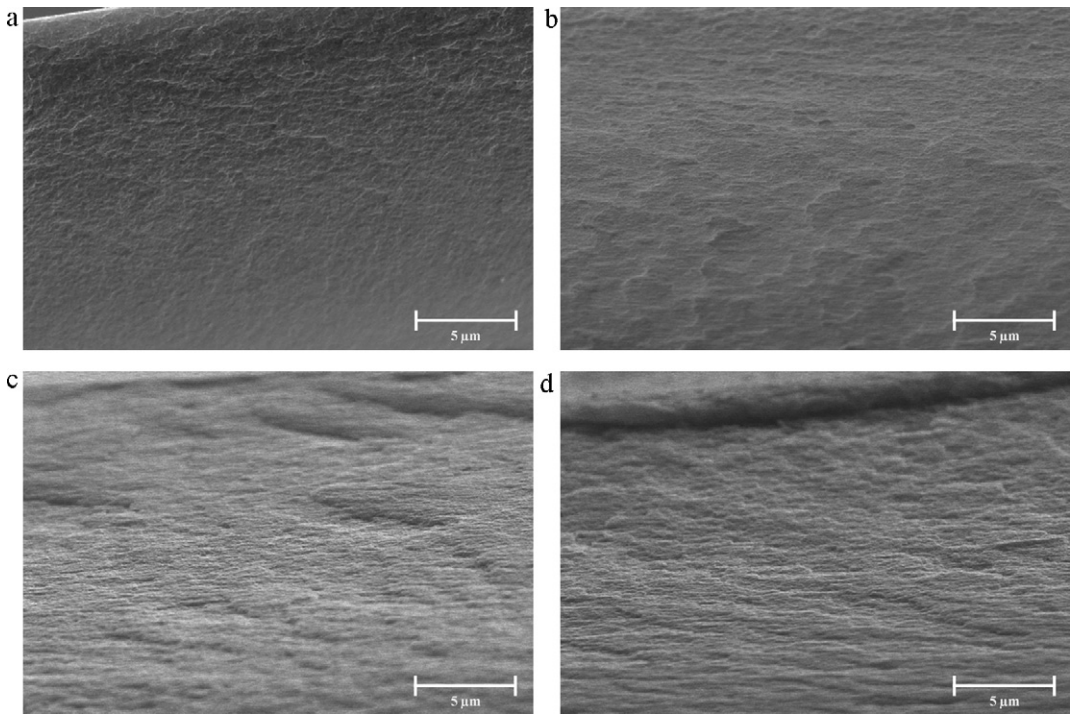

Fig. 4. The fractured surfaces of the (a) pure cellulose film and the GO ((b) 1 wt%, (c) 3 wt%, (d) 5 wt%)/cellulose composite films.

ever, the *d*-spacing representing the in-plane hexagonal structure did not change as compared to that of the graphite (2.1 Å). These results indicate that the GO, which was intercalated by introducing the oxygen containing groups, was oriented with its large surface of the carbon sheet parallel to the surface of the GO film and the basic hexagonal in-plane structure of the graphite maintained during oxidation, even though many defects in the carbon sheet existed through oxidation. The two-dimensional X-ray patterns of the pure cellulose and the GO (5 wt%)/cellulose composite films (Fig. 3c and d) show the identical broad peaks at $2\theta = 12.0^\circ$ (*d*-spacing = 7.4 Å) and 21.5° (*d*-spacing = 4.1 Å), which can be indexed as $1\,\bar{1}\,0$ and 110 + 200 of the cellulose II crystal, respectively, the unit cell dimensions are $a = 8.01$ Å, $b = 9.04$ Å, $c = 10.36$ Å, and $\gamma = 117.1^\circ$ (Kolpak & Blackwell, 1976). The $1\,\bar{1}\,0$ reflection was preferentially oriented perpendicularly to the film for both patterns indicating that a uniplanar orientation of the cellulose crystal was produced during film casting with a $1\,\bar{1}\,0$ plane parallel to the film surface. The cellulose chains are known to be tightly connected by intermolecular hydrogen bonds in the $1\,\bar{1}\,0$ planes so that the hydrogen-bonded sheets could be aligned parallel to the film's surface with normal force during film casting. However, any traces of the intercalated GO at $2\theta = 12.2^\circ$ were not found in the X-ray patterns of the GO (5 wt%)/cellulose composite film indicating that the completely exfoliated structure was made in the composite film. Thus, the mechanical stirring and sonication during the dope preparation was enough to exfoliate the intercalated GO in the composite.

Fig. 4a–d shows the fractured surfaces of the pure cellulose and the GO (1, 3, 5 wt%)/cellulose composite films in liquid nitrogen. The fractured surfaces of the pure cellulose and all studied composite films were smooth, without any aggregations of the GO, indicating that the exfoliated GOs (graphene oxides) were well dispersed in the cellulose matrix. However, the texture of the fractured surface became anisotropic as the ϕ increased due to the parallel orientation of the carbon sheets of the GO against the film's surface.

3.3. Properties of the GO/cellulose composite

Fig. 5a shows the TGA thermograms of the composite films at different ϕ_s. All GO/cellulose composites were degraded at ~320 °C, regardless of ϕ, while the carbonaceous residues, at 500 °C, increased as the ϕ increased as shown in Fig. 5b. The residues increased rapidly until $\phi = 1$ wt% but gradually increased after that. The residues produced were more than the combined amount of the input GO and the residue from the pure cellulose. For example, the residue at $\phi = 0$ wt% (the pure cellulose) was 20.5 wt% but at $\phi = 0.25$ wt% was 24.5 wt%. It was reported that significant interactions between cellulose and lignin during the carbonization contributed in the increases in carbonization yields during the carbonization (Saeed & Park, 2007a,b). Thus, the interactions between cellulose and the GO might induce an increase in the carbonization of the cellulose at the interface between the GO and cellulose. However, the interfacial regions between the GO and cellulose might begin to overlap at $\phi = 1$ wt% so that the increase rate of the carbon residues decreased with further increases of ϕ. The increase of carbonaceous residue of cellulose might be a positive factor for its use as a carbon fiber precursor because cellulose fibers have been known to have a low carbon yield during carbonization as compared to polyacrylonitrile (PAN) fibers. The weight loss at ~ 230 °C was noticeable and its temperature was close to the temperature at which a major weight loss of the GO occurred due to the removal of the oxygen-containing groups.

Fig. 6 shows the change of the electrical conductivities of the GO/cellulose composite films as a function of ϕ with and without annealing at 250 °C for 30 min. The electrical conductivity of the GO/cellulose films, without annealing, continuously increased as ϕ increased. However, the conductivity levels were less than 10^{-5} S cm^{-1} because the GO was a nearly non-conducting material. The electrical conductivities increased by annealing the composite films. For example, the electrical conductivity increased approximately two orders from ~10^{-6} S cm^{-1} to ~10^{-4} S cm^{-1} at $\phi = 5$ wt% after annealing. Thermal annealing could remove the

Table 1
The change of mechanical properties of the composite films at different ϕ_s.

ϕ (wt%)	Tensile properties			
	Young's modulus (MPa)	Tensile strength (MPa)	Elongation at break (%)	Toughness (MPa)
0	4530.9 ± 639.7	73.1 ± 10.1	15.8 ± 1.3	9.4 ± 1.3
0.25	5479.5 ± 471.8	87.4 ± 10.2	5.8 ± 2.0	3.8 ± 2.0
0.5	5316.3 ± 63.4	84.9 ± 2.2	5.9 ± 0.8	3.8 ± 0.7
0.75	5876.2 ± 1913.6	87.4 ± 2.8	8.1 ± 1.2	5.6 ± 1.2
1	4749.0 ± 71.8	84.2 ± 2.0	7.3 ± 1.3	4.8 ± 1.1
3	4525.8 ± 300.1	80.8 ± 2.1	5.1 ± 1.1	3.1 ± 0.9
5	5478.4 ± 194.1	97.8 ± 8.2	6.1 ± 1.1	4.4 ± 1.2

oxygen-containing groups of the GO in the composite. A high temperature annealing method has been known to be effective in deoxygenating the GO and restoring its conductivity. The X-ray photoelectron spectroscopy measurements of the GO showed that the percentage of oxygen-containing functional groups dramatically decreased during annealing, even at 220 °C. We also found a small reduction in weight at ~230 °C in Fig. 5 due to the removal of the labile oxygen-containing groups. The annealing temperature of 250 °C was below the degradation temperature of the cellulose (320 °C) and above the temperature for removing oxygen-containing groups so that the increase of conductivity could be observed.

Table 1 shows the change of mechanical properties of the composite films at different ϕ_s. Young's modulus and tensile strength of the composite films increased by adding the GO into the cellulose; Young's modulus and tensile strength increased 31% and 19%, respectively, at ϕ = 0.75 wt% as compared to those at ϕ = 0 wt% (pure cellulose). However, the elongation at break decreased by adding the GO into the cellulose; a maximum of 68% decreased at ϕ = 3 wt% as compared to pure cellulose. The interactions between the GO and cellulose made the composite films stronger but brittle. This was achieved by adding a small amount of GO into the composite.

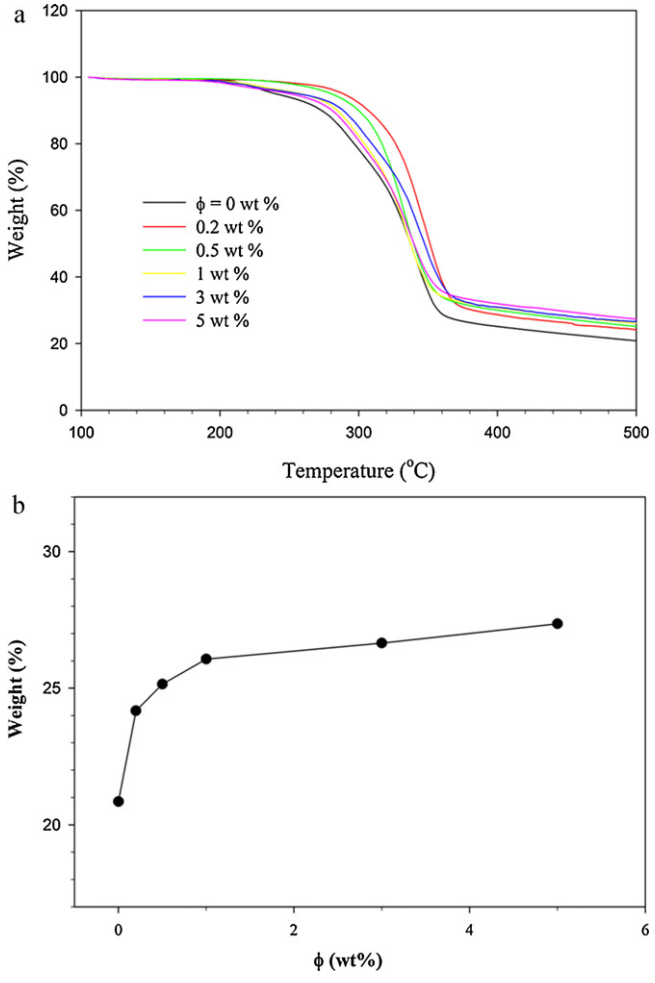

Fig. 5. (a) TGA thermograms of the GO/cellulose composite films at different ϕ_s, and (b) the carbonaceous residue at 500 °C as a function of ϕ.

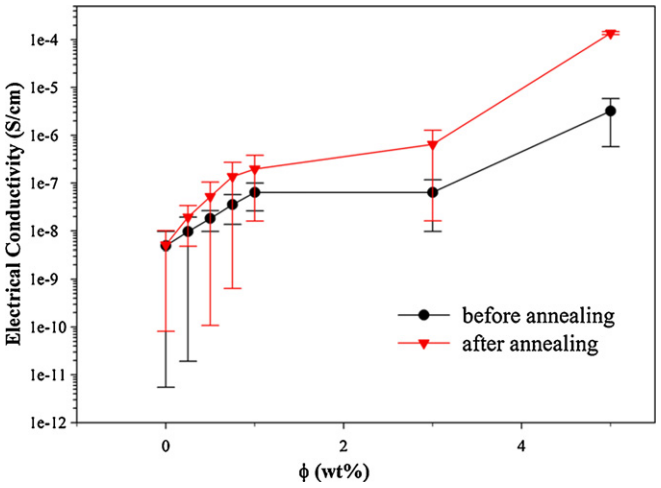

Fig. 6. Electrical conductivity as a function of ϕ with and without annealing at 250 °C for 30 min.

4. Conclusion

The GO was dispersed well in NMMO through mechanical treatments, such as sonication and mechanical stirring, which led to the exfoliation of the GO into individually separated carbon sheets (graphene oxide). The GO/NMMO solution dissolved cellulose completely to make the GO/NMMO/cellulose dope which was cast and coagulated into a composite film in which the graphite oxide was dispersed in the state of GO without any aggregation. The interactions between the GO and NMMO caused enhanced viscosity by adding a small amount of the GO (less than 0.75 wt%) into the dope through the increased elastic property. The GO/cellulose composite film showed improved thermal, mechanical, and electrical properties through the presence of a small amount of GO in the composite, which might have strong hydrogen bonds between the GO and cellulose. The electrical conductivity of the composite was improved by annealing the composite film at a relatively low temperature (220 °C) probably due to the removal of the oxygen-containing groups of the GO in the composite. More carbonaceous residues of the composite films were produced after the TGA experiment as compared to that of the pure cellulose and might be a positive factor for use as a carbon fiber precursor. We found that this solution-blend composite system, having hydrogen bonding capabilities among matrix (cellulose), filler (GO), and solvent (NMMO),

was demonstrated to be a good model system for dispersing and exfoliating the GO in the composite.

Acknowledgements

Financial support from Asian Office of Aerospace Research and Development through Air Force Research Laboratory (AOARD-10-4081) is gratefully acknowledged.

References

Balandin, A. A., Ghosh, S., Bao, W. Z., Calizo, I., Teweldebrhan, D., Miao, F., et al. (2008). Superior thermal conductivity of single-layer graphene. *Nano Letters*, *8*(3), 902–907.

Berger, C., Song, Z. M., Li, X. B., Wu, X. S., Brown, N., Naud, C., et al. (2006). Electronic confinement and coherence in patterned epitaxial graphene. *Science*, *312*(5777), 1191–1196.

Castro, N., Guinea, F., Peres, N. M. R., Novoselov, K. S., & Geim, A. K. (2009). The electronic properties of graphene. *Reviews of Modern Physics*, *81*(1), 109–162.

Chung, D. D. L. (2004). Review: Electrical applications of carbon materials. *Journal of Materials Science*, *39*(8), 2645–2661.

Eda, G., Fanchini, G., & Chhowalla, M. (2008). Large-area ultrathin films of reduced graphene oxide as a transparent and flexible electronic material. *Nature Nanotechnology*, *3*(5), 270–274.

Geim, A. K., & Novoselov, K. S. (2007). The rise of graphene. *Nature Materials*, *6*(3), 183–191.

Han, M. Y., Oezyilmaz, B., Zhang, Y., & Kim, P. (2007). Energy band-gap engineering of graphene nanoribbons. *Physical Review Letters*, *98*(20), 206805 (1–4).

Hirata, M., Gotou, T., Horiuchi, S., Fujiwara, M., & Ohba, M. (2004). Thin-film particles of GO. 1. High-yield synthesis and flexibility of the particles. *Carbon*, *42*(14), 2929–2937.

Hirata, M., Gotou, T., & Ohba, M. (2005). Thin-film particles of GO. 2. Preliminary studies for internal micro fabrication of single particle and carbonaceous electronic circuits. *Carbon*, *43*(3), 503–510.

Klemm, D., Heublein, B., Fink, H. P., & Bohn, A. (2005). Cellulose: Fascinating biopolymers and sustainable raw material. *Angewandte Chemie International Edition*, *44*(22), 3358–3393.

Kolpak, F. J., & Blackwell, J. (1976). Determination of the structure of cellulose II, 9(2), 273–278.

Lee, C., Wei, X., Kysar, J. W., & Hone, J. (2008). Measurement of the elastic properties and intrinsic strength of monolayer graphene. *Science*, *321*(5887), 385–388.

Li, D., Muller, M. B., Gilje, S., Kaner, R. B., & Wallace, G. G. (2008). Processable aqueous dispersions of graphene nanosheets. *Nature Nanotechnology*, *3*(2), 101–105.

Liu, Q., Liu, Z. F., Zhang, X. Y., Zhang, N., Yang, L. Y., Yin, S. G., et al. (2008). Organic photovoltaic cells based on an acceptor of soluble graphene. *Applied Physics Letters*, *92*(22), 223303 (1–3).

Mori, T., Kikuzawa, Y., & Takeuchi, H. (2008). N-type field-effect transistor based on a fluorinated-graphene. *Organic Electronics*, *9*(3), 328–332.

Novoselov, K. S., Geim, A. K., Morozov, S. V., Jiang, D., Zhang, Y., Dubonos, S. V., et al. (2004). Electric field effect in atomically thin carbon films. *Science*, *306*(5696), 666–669.

Novoselov, K. S., Geim, A. K., Morozov, S. V., Jiang, D., Katsnelson, M. I., Grigorieva, I. V., et al. (2005). Two-dimensional gas of massless Dirac fermions in graphene. *Nature*, *438*(10), 197–200.

Paredes, J. I., Villar-Rodil, S., Martinez-Alonso, A., & Tascon, J. M. D. (2008). Graphene oxide dispersions in organic solvents. *Langmuir*, *24*(19), 10560–10564.

Ramanathan, T., Abdala, A. A., Stankovich, S., Dikin, D. A., Herrera-Alonso, M., Piner, R. D., et al. (2008). Functionalized graphene sheets for polymer composites. *Nature Nanotechnology*, *3*(6), 327–331.

Saeed, K., & Park, S. Y. (2007a). Preparation of multiwalled carbon nanotube/nylon-6 nanocomposites by in situ polymerization. *Journal of Applied Polymer Science*, *106*(6), 3729–3735.

Saeed, K., & Park, S. Y. (2007b). Preparation and properties of multiwalled carbon nanotube/polycaprolactone nanocomposites. *Journal of Applied Polymer Science*, *104*(3), 1957–1963.

Schedin, F., Geim, A. K., Morozov, S. V., Hill, E. W., Blake, P., Katsnelson, M. I., et al. (2007). Detection of individual gas molecules adsorbed on grapheme. *Nature Materials*, *6*(9), 652–655.

Stankovich, S., Dikin, D. A., Dommett, G. H. B., Kohlhaas, K. M., Zimney, E. J., Stach, E. A., et al. (2006). *Nature London*, *442*(7100), 282–286.

Stankovich, S., Piner, R. D., Nguyen, S. T., & Ruoff, R. S. (2006). Synthesis and exfoliation of isocyanate-treated graphene oxide nanoplatelets. *Carbon*, *44*(15), 3342–3347.

Stankovich, S., Dikin, D. A., Piner, R. D., Kohlhaas, K. A., Kleinhammes, A., Jia, Y., et al. (2007). Synthesis of graphene-based nanosheets via chemical reduction of exfoliated GO. *Carbon*, *45*(7), 1558–1565.

Sutter, P. W., Flege, J. I., & Sutter, E. A. (2008). Epitaxial graphene on ruthenium. *Nature Materials*, *7*(5), 406–411.

Szabo, T., Szeri, A., & Dekany, I. (2005). DRIFT study of deuterium-exchanged GO. *Carbon*, *43*(15), 3186–3189.

Szabo, T., Berkesi, O., Forgo, P., Josepovits, K., Sanakis, Y., Petridis, D., et al. (2006). Evolution of surface functional groups in a series of progressively oxidized GOs. *Chemistry of Materials*, *18*(11), 2740–2749.

Vivekchand, S. R. C., Rout, C. S., Subrahmanyam, K. S., Govindaraj, A., & Rao, C. N. R. (2008). Graphene-based electrochemical supercapacitors. *Journal of Chemical Sciences*, *120*(1), 9–13.

Wang, X., Zhi, L. J., & Mullen, K. (2008). Transparent conductive grapheme electrodes for dye-sensitized solar cells. *Nano Letters*, *8*(1), 323–327.

Wang, X., Zhi, V., Tsao, N., Tomovic, Z., Li, J. L., & Mullen, K. (2008). Transparent carbon films as electrodes in organic solar cells. *Angewandte Chemie International Edition*, *47*(16), 2990–2992.

Wu, Z. S., Pei, S., Ren, W., Tang, D., Gao, L., Liu, B., et al. (2009). Field emission of single-layer graphene films prepared by electrophoretic deposition. *Advanced Materials*, *21*(17), 1756–1760.

Yoo, E. J., Kim, J. D., Hosono, E., Zhou, H., Kudo, T., & Honma, I. (2008). Large reversible Li storage of graphene nanosheet families for use in rechargeable lithium ion batteries. *Nano Letters*, *8*(8), 2277–2282.

Zhang, Y. B., Tan, Y. W., Stormer, H. L., & Kim, P. (2005). Experimental observation of the quantum Hall effect and Berry's phase in graphene. *Nature*, *438*(10), 201–204.

Zhang, Q., Rastogi, S., Chen, D., Lippits, D., & Lemstra, P. J. (2006). Low percolation threshold in single-walled carbon nanotube/high density polyethylene composites prepared by melt processing technique. *Carbon*, *44*(4), 778–785.